Vitamin C for photo-stable non-fullerene-acceptor based organic solar cells

Sambathkumar Balasubramanian*, Miguel-Angel Leon-Luna, Beatriz Romero Herrero, Morten Madsen, Vida Turkovic*

*Corresponding authors: sambathkumar@mci.sdu.dk, engmann@mci.sdu.dk

Since recently, with the advent of the new class of molecules, the so-called non-fullerene acceptors', the power conversion efficiencies of organic solar cells have skyrocketed. However, rapid degradation occurs under illumination, particularly when ZnO is used as the electron transport layer in these devices. We introduced vitamin C (ascorbic acid) into the organic solar cells as a photostabilizer, and systematically studied its photostabilizing effect on inverted PBDBT:IT-4F devices. The presence of vitamin C as an antioxidant layer between ZnO and the photoactive layer strongly suppressed the photocatalytic effect of ZnO that induces NFA photodegradation. Upon 96 h of exposure to AM 1.5G 1 Sun irradiation, the reference devices lost 62 % of their initial efficiency, while those containing vitamin C lost only 36 %. The UV-visible absorption, impedance spectroscopy, and light-dependent voltage and current measurements reveal that vitamin C reduces the photobleaching of NFA molecules and also suppresses the charge recombination. This simple approach using a low-cost, naturally occurring antioxidant, provides an efficient strategy for improving photostability of organic semiconductor based devices.

1. Introduction

Organic solar cells (OSC) have emerged as a promising photovoltaic technology, having the advantage of solution processability that makes them compatible with cost-effective roll-to-roll printing process that can be applied on thin flexible substrates.[1] It offers a wide variety of applications such as agrivoltaics, Internet of Things (IOT), wearable electronics and semi-transparent windows.[2] To date, OSC have reached a power conversion efficiency (PCE) of over 19 %, boosted by the development of novel non-fullerene acceptors (NFA).[3] However, stability of these devices still requires optimization. A lot of effort has been made to understand the degradation mechanisms, in order to improve the device stability and lifetime.[4] So far

various degradation mechanisms have been identified, and the main stress factors include UV-vis irradiation, heat, oxygen and humidity. Penetration of humidity and oxygen leads to a serious degradation of the active layer, interface layers and the electrodes, and the degradation factor can be accelerated in the presence of UV-vis irradiation. This type of degradation can be avoided or slowed down by proper encapsulation.[5] The other major issue that affects the devices' lifetime is poor photostability under constant UV-vis irradiation, even in nitrogen-controlled conditions.[6] It has been reported that NFA OSC show excellent photostability under white LED light (without UV part), with an extrapolated T_{80} lifetime of 10 years. [7] But it is still challenging to achieve good photostability for NFA OSC under air mass (AM) 1.5 illumination spectrum (100 mW cm^{-2}) which contains a small amount of UV light (2 mW cm^{-2}).[7]

Zinc oxide (ZnO) is commonly used as an electron transport layer (ETL) in inverted NFA OSC, because of its high optical transparency, well-matched work function and Conduction Band Minimum (CBM), sufficient n-type character with charge carrier selectivity (low lying valence band), low cost, easy synthesis and simple solution processability.[8] Despite these advantages, ZnO ETL undergoes photocatalytic reactions which lead to decomposition and photooxidation of organic molecules (and NFA) on the surface of ZnO via redox reactions and formation of hydroxyl radicals [7c]. This subsequently leads to charge accumulation and recombination at the ZnO interface, which both strongly reduce the device stability.[7a, 9, M. Ahmadpour et al under review (2023)].Various approaches have been explored to control interfacial degradation: Su and co-workers utilized nitrogen and sulfur-doped graphene oxide nanosheets (NS-GNS) as a modifier layer for ZnO[10], Hu et al. used aqueous polyethylenimine as a modifier layer[11], Liu et al. developed modified ZnO layers, Me-ZnO, DMSO-ZnO, and sol-gel-ZnO[12], Xu et.al used C_{60} self-assembled monolayer (SAM) as a protective buffer layer[13]. Recently, U. K. Aryal et al. demonstrated that 2D Mxene could be embedded with ZnO to reduce this photocatalytic decomposition on ZnO surface [U. K. Aryal et al. under review (2023)] In this work, we investigate the stabilization effect using an antioxidant interlayer between ZnO and active layer.

We have previously demonstrated a successful new pathway of stabilizing organic solar cells by introducing antioxidants as the third component in the active layer, which interferes with the photooxidation process by deactivating the reactive oxygen species (ROS), by scavenging radicals, or by acting as a barrier to UV irradiation. [14] Recently, we have reported an improved photostability for OSC devices using naturally occurring antioxidant molecule, β-

carotene, as an effective quencher of singlet oxygen and its precursors.[15] We also demonstrated a rapidly improved devices' lifetime using a multifunctional additive, consisting of another carotenoid antioxidant, astaxanthin, covalently bonded to an polymeric organosilicon, which at the same time increase the photooxidative stability of the devices and improve their mechanical integrity[16]. This antioxidant-assisted stabilization approach has been as well reported effective in NFA-based active layers[17].

In this work we use a naturally occurring antioxidant material, vitamin C (ascorbic acid), as an ultrathin interlayer that suppresses the ZnO-influenced photocatalytic degradation of NFA-based active layers, resulting in extended stability of the devices. We found that vitamin C as an interlayer significantly suppresses the photobleaching of IT-4F, as evident from UV-vis absorption spectroscopy. Impedance spectroscopy (IS) analysis revealed higher recombination resistance values (R_{rec}) for vitamin C based devices, which can be attributed to lower recombination losses as compared to the reference devices. Consequently, vitamin C-based devices showed better photostability, maintaining 64 % of their original value even after 96 h, as compared to reference devices which retain only 38 %.

2. Results and Discussion

2.1 Device Properties

Vitamin C is a potent reducing agent that has a very low redox potential, which enables it to react with almost all oxidizing free radicals, among them also the hydroxyl radical [7c] and superoxide radical anion[18] which are known to be photooxidative intermediates in most NFA molecules .[19] It is found at high concentrations in many animal tissues and plants[20], and it is also extensively used as an antioxidant in a great variety of products and food industry. [21] In this work we systematically analyze the stabilizing effect of vitamin C on PBDBT:IT-4F:IT-4F (Poly[(2,6-(4,8-bis(5-(2-ethylhexyl) thiophen-2-yl)-benzo[1,2-b:4,5-b']dithiophene))-alt-(5,5-(1',3'-di-2-thienyl-5',7'-bis(2-ethylhexyl)benzo[1',2'-c:4',5'-c']dithiophene-4,8-dione)] : 3,9-bis(2-methylene-((3-(1,1-dicyanomethylene)-6,7-difluoro)-indanone))-5,5,11,11-tetrakis(4-hexylphenyl)-dithieno[2,3-d:2',3'-d']-s-indaceno[1,2-b:5,6-b']dithiophene) organic solar cells.
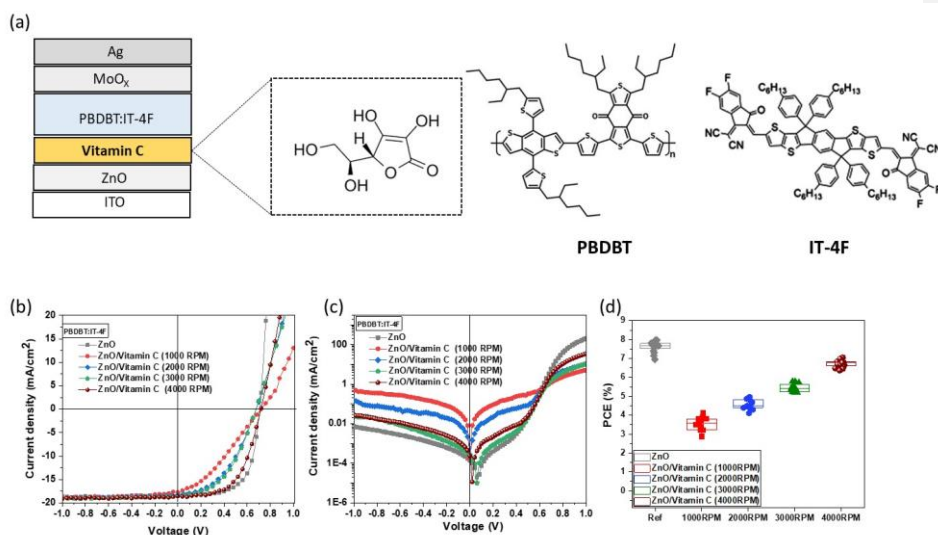
Figure 1. (a) Inverted device layer stack and molecular structures of vitamin C, PBDBT and IT-4F, (b, c) Light and Dark J-V characteristics of PBDBT:IT-4F devices in linear and semilogarithmic scale, (d) Histogram of PBDBT:IT-4F device with ZnO and the ZnO modified with vitamin C.

Table 1. Solar cell parameters of PBDBT:IT-4F devices with different thicknesses of vitamin C as the interfacial layer between ZnO and active layer. The values in the parentheses are the average values obtained for 12 devices.

Interface layer	V_{OC} [V]	J_{SC} [mA/cm^2]	FF [%]	PCE [%]
ZnO	0.70	18.3	62.1	8.0
	(0.69±0.01)	(17.9±0.4)	(61.7±0.7)	(7.6±0.3)
ZnO/Vitamin C (1000 rpm)	0.72	17.7	32.5	4.1
	(0.69±0.02)	(17.6±0.3)	(31.5±1.4)	(4.0±0.4)
ZnO/Vitamin C (2000 rpm)	0.68	18.3	44.2	5.5
	(0.69±0.01)	(18.0±0.3)	(43.7±1.8)	(5.4±0.4)
ZnO/Vitamin C (3000 rpm)	0.68	18.5	46.3	5.8
	(0.69±0.01)	(18.2±0.3)	(45.8±0.9)	(5.8±0.2)
ZnO/Vitamin C (4000 rpm)	0.70	18.6	56.1	7.3
	(0.69±0.02)	(18.3±0.4)	(55.6±1.3)	(7.1±0.4)

First, we optimized the thickness of vitamin C interlayer by dissolving 2 mg of vitamin C in 1 mL of ethanol and spin coating it at different speeds on ZnO. The device architecture employed was indium tin oxide (ITO)/ZnO/vitamin C/PBDBT:IT-4F/MoOx/Ag (**Figure 1a**). The chemical structures of the donor and acceptor molecules are also shown in **Figure 1a**. Their corresponding light and dark current density-voltage (J-V) curves, measured under AM 1.5G light intensity (100 mW/cm^2), are shown in **Figure 1b** and **1c,** and their corresponding solar cell parameters are summarized in **Table 1**. With the increasing spin speed from 1000 to 4000 rpm, i.e., decrease in thickness of vitamin C layer, the PCE increases from 4.11 to 7.31 %. This improvement in device performance is directly correlated with FF. The best device efficiency of 7.31 %, with a V_{oc} of 0.7 V, J_{sc} of 18.61 mA/cm^2, and FF of 56 %, was achieved for devices with the thinnest vitamin C layer (4000 rpm), which is only marginally lower than the control device (PCE = 7.97 %, V_{oc} = 0.7 V, J_{sc} = 18.33 mA/cm^2 and FF = 62 %). The vitamin C devices exhibited initial "S"-shaped J-V characteristics, which was rectified upon several minutes of light soaking, from 4.10 % to 7.28 % (see **Figure S1** and **Table S1)**. The EQE spectra are shown in **Figure S2.** Both control and vitamin C devices show strong photoresponse from 500 to 750 nm with a similar profile, and the trend is well correlated with the J-V curves. From the semilogarithmic dark J-V curves, shown in **Figure 1c**, it can be seen that the reference and vitamin C (4000 rpm) devices suffer from less leakage current and yield a higher injection current density under reverse and forward bias. This can be attributed to a lower injection barrier between the interface and active layer, which correlates well with the light J-V characteristics.[23] A histogram of PCE is shown in **Figure 1d**, and J_{sc}, V_{oc} and FF are displayed in **Figure S3**. The PCE follows the same tendency as FF, increasing as the layer becomes thinner. Based on this, for the further studies, we focus on the devices containing vitamin C layer made by spin coating at 4000 rpm.

2.2 Photostability improvement of OSC in the presence of vitamin C
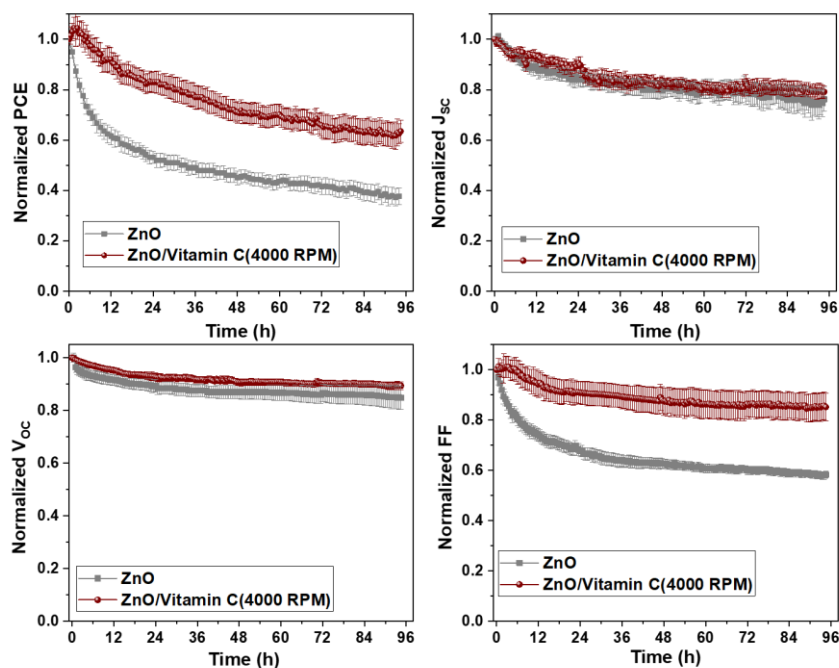

Figure 2. Evolution of solar cell parameters (PCE, FF, J_{sc}, and V_{oc}) of encapsulated PBDBT:IT-4F devices without and with vitamin C interlayer, under continuous 1 Sun AM 1.5G irradiation in ambient atmosphere at 35°C. Data points represent the average over twelve devices, normalized with respect to the initial data point, with the standard deviations as the error bar.

Table 2. Summary of degradation parameters of PBDBT:IT-4F devices, reference and with vitamin C interlayer, under AM 1.5G irradiation at 100 mW cm^{-2} in N$_2$. For extracted parameters of the bi-exponential fit and the fitting errors, see Table S2.

	$t_{burn\text{-}in}$[h]	$PCE_{burn\text{-}in}$[%]	PCE_{80}[%]	t_{80}[h]	$t_{lifetime}$[h]	$PCE_{initial}$[%]	$PCE_{burn\text{-}in}/PCE_{initial}$[%]	$APG_{lifetime}$[kWhm^{-2}]
Reference	22.7	3.1	2.5	64.2	41.5	5.6	55.6	1.4
Vitamin C	29.9	3.9	3.1	81.5	51.6	5.1	76.6	2.1

The photostability of encapsulated devices was tested in a lifetime setup with automated measurements at every 30 minutes under open circuit conditions. **Figure 2** and **Table 2.** compare the evolution of PCE, FF, J_{SC} and V_{OC} of encapsulated devices without and with vitamin C interlayer, under continuous exposure to 1 Sun UV-vis irradiation. The PCE evolution of reference devices, containing pure ZnO ETL, suffers from a strong burn-in of 44 % in magnitude, as compared to the vitamin C devices that loses only 23 %. Also, the burn-in dynamics are slowed down in presence of vitamin C – its duration is 29.9 h, as compared to the reference burn-in period of 22.7 h. The same improvement is seen in T_{80} - the reference devices reach it after 64.2 h, and vitamin C devices after 81.5 h. It is to note that over the duration of this experiment of 96 hours, the vitamin C devices retained 64 % of their original PCE, while the reference devices retained only 38 %. Thus, the presence of vitamin C resulted in an overall 50 % increase of the accumulated power generation (APG) over the lifetime of the devices. The PCE decay of reference devices originates mainly from a reduction in FF ($\approx$ 40 %), with the additional contribution of J_{SC} ($\approx$ 20 %) and V_{OC} ($\approx$ 15 %). All of the vitamin C-treated devices, regardless of the thickness (i.e., spin speeds of 1000, 2000, 3000 and 4000 rpm) resulted in a higher photostability as compared to the reference devices that contain pure ZnO ETL, as shown in **Figure S4**.
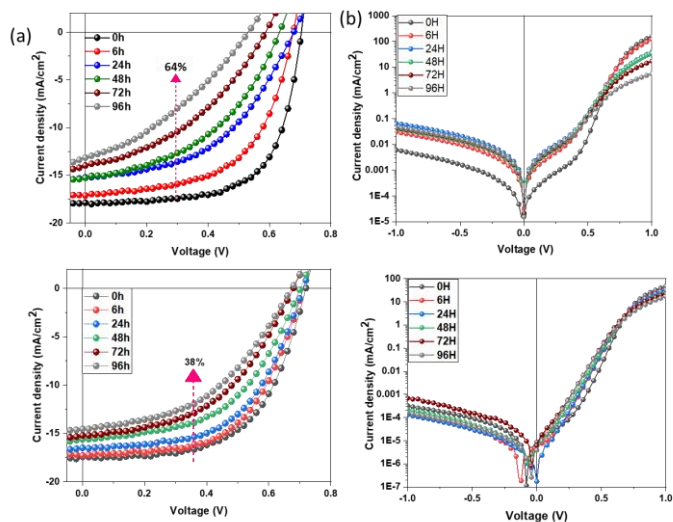

Figure 3. (a, c) Light (J-V) & (b, d) Dark (J-V) plots of reference ZnO and ZnO/vitamin C (4000 rpm) encapsulated devices under continuous exposure to 1 Sun AM 1.5G in ambient atmosphere at 35°C for different durations of up to 96 h.

Figure 3a and **3c** show the light J-V characteristics of reference and devices with vitamin C at different stages of photodegradation. We can observe a strong trend in reference devices, leading up to a 5-fold increase in series resistance and a decrease in the shunt resistance over the time of exposure. This suggests a weakening of bulk conductivity and a decrease of charge selectivity. Under the same conditions, the devices containing the vitamin C interlayer are much less affected, as shown in **Table S3**. To further understand the degradation nature, dark J-V characteristics were measured and their semilogarithmic plots are shown in **Figure 3b** and **3d**. The dark J-V curves of the reference devices show a significantly higher leakage current in reverse bias over the exposure time, as compared to devices with vitamin C interlayer, exhibiting weaker diode characteristics. In addition, the slope value near the injection region (0.5 V to 1 V) is for the reference devices decreasing over time, indicating the light-induced loss of ETL functionality of ZnO, which is strongly reduced in devices containing vitamin C interlayer.[23]

2.3 UV-vis stability of pristine and blend films

To further understand the photostabilizing effect of vitamin C on the PBDBT:IT-4F devices, the absorption measurements were recorded on films of IT-4F, PBDBT and PBDBT:IT-4F blend, deposited on bare glass, glass coated with ZnO, and glass coated with ZnO and vitamin C, as shown in **Figure 4**. The films were stored in N_2 atmosphere under 1 Sun AM 1.5G irradiation, and the UV-vis spectra were recorded periodically for up to 80 h of exposure. As shown in **Figure 4 (a-c),** IT-4F film undergoes a fast loss of absorption, decaying down to 20 % of initial absorption upon 80 h (**Figure S5 b**). As evident from **Figure 4 (g-i)**, the same trend can be observed in blend films, and at a strongly reduced magnitude also in pristine PBDBT films (largest loss on ZnO of only ≈5 %, as evident from **Figure S5 a**). This can be attributed to the ZnO photocatalytic activity, in which a photoexcited ZnO produces electron-hole pairs that take part in redox reactions in contact with humidity and oxygen and hydroxide ions, to produce hydroxyl radicals and superoxide radical anions, which are strong oxidizing agents [24] known to readily react and degrade the OPV molecules.[19, 25, 7c] In comparison, IT-4F films in absence of ZnO do not suffer from such strong losses. The same can be achieved in presence of ZnO when a vitamin C interlayer is inserted in between, in which case vitamin

C shields the organic molecules from the radical attack originating from ZnO, and thus clearly mitigates this degradation effect.
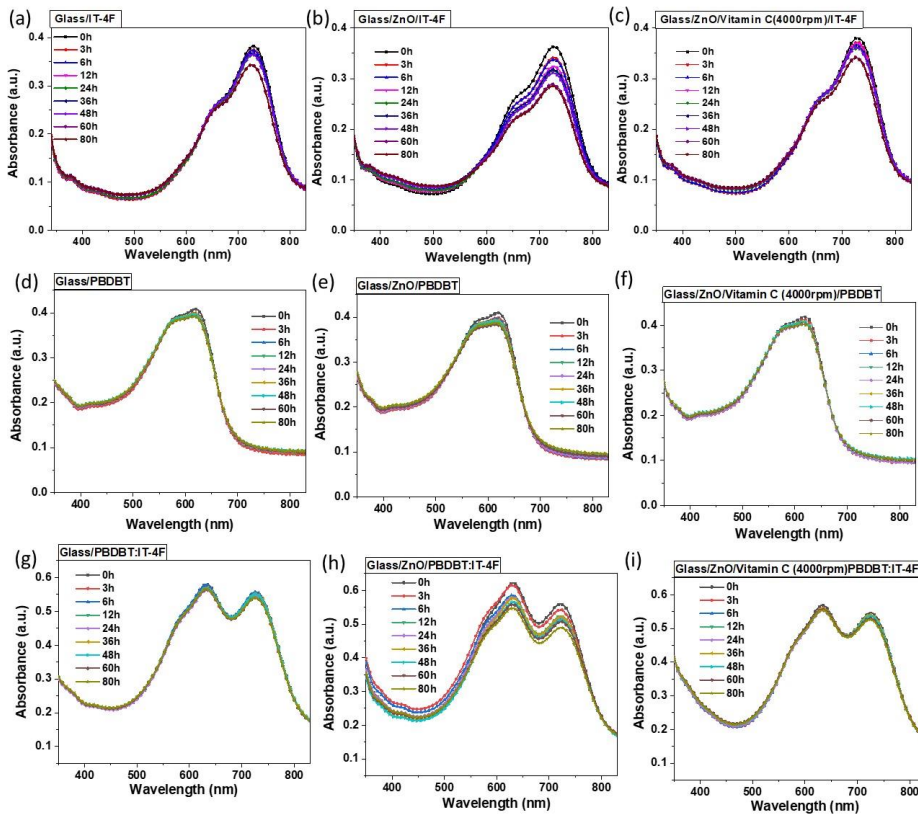

Figure 4. UV-vis absorption spectra of IT-4F (a-c); PBDBT (d-f); PBDBT:IT-4F (g-i) under continuous exposure to AM 1.5G 1 Sun irradiation in N_2 atmosphere at 35°C.

2.4 Recombination analysis using impedance and light intensity dependent measurements

To investigate the effect of the degradation on the electrical characteristics of OSC in presence of vitamin C, Impedance Spectroscopy (IS) measurements were carried out. The measurements were conducted in dark conditions, at 0 V applied potential, with the frequency ranging from 10 Hz to 1 MHz, and 10 mV amplitude.[26] The Nyquist plots of reference devices and devices with vitamin C interlayer, under exposure to, up to 96 hours, of 1 Sun AM 1.5G irradiation, are

presented in **Figure 5** (**a, b**). The results were fitted using an equivalent-circuit model (ECM) shown in **Figure S6**. The decrease in the semi-circle radii as the devices are degraded is explained by the decrease in the charge recombination resistance (R_{rec}) according to the model employed.[10] **Table 2** tracks the progression of the fitted non-radiative recombination resistance values for reference devices and devices containing vitamin C interlayer upon exposure to 1 Sun AM 1.5G irradiation for up to 96 hours. From the table (also refer to **Figure S7**) it is clear that reference devices undergo a significant reduction in R_{rec} value (≈ 80 % loss at 96 h), while the devices containing vitamin C interlayer lose only 50 % at the same time. This clearly shows that the reference devices, in which the ZnO ETL is in direct contact with the PBDBT:IT-4F active layer, suffer from severe charge recombination increase upon exposure to light. In addition, the initial R_{rec} value for devices containing a vitamin C interlayer is two orders of magnitude higher than that of the reference devices, indicating that vitamin C suppresses the recombination. The suppression of defects with vitamin C was further verified using the capacitance measurements.

To quantify the change in the built-in electric field (V_{BI}) for fresh and photodegraded devices, capacitance-voltage measurements were carried out on reference devices and devices containing vitamin C interlayer. The related (C^{-2}–V) curves of the fresh and aged devices are shown in **Figure 5 (c, d).** The built-in potential (V_{Bi}) was calculated by the Mott-Schottky equation: [26]

$$C_{sc}^{-2} = 2(V_{BI}-V)/(A^2 q \varepsilon_r \varepsilon_0 N_A)$$

where C_{sc} is the value of the capacitance of the space-charge region, V the applied voltage, q the elementary charge, A the device area, ε_r and ε_0 the relative dielectric constant estimated by the geometric capacitance measured at 10 kHz at 0 V and the vacuum permittivity, respectively (see **Table S4**). For organic semiconductors, the above equation can be applied assuming that the defect states are the only contributors of charge carriers in the depletion layer of the p-n junction. Thus, N_A corresponds to the density of defects.[26,27] For more information on the calculation of the relative dielectric constant, please see SI. The respective values are tabulated in **Table 3**. As shown in **Figure 5 (e, f),** the V_{Bi} value of reference devices drops over time under light stress from 0.572 to 0.540 V (≈ 5 % loss). Meanwhile, under the same conditions, in the devices with vitamin C interlayer, the decrease in V_{BI} is lower (≈ 3 % loss, from 0.568 to 0.549 V). This relation is in good agreement with the observed V_{OC} drop in the lifetime measurements (see **Figure 2**). N_A value raises in both reference and vitamin C devices and

reaches similar values, however, the rise of N_A in the initial period (after 24 h) is much steeper for reference devices (from 1.43×10^{20} to 2.86×10^{20} cm^{-3}), as compared to vitamin C devices (from 1.33×10^{20} to 1.86×10^{20} cm^{-3}). The latter indicates that the reference devices degrade faster. This is in accordance with the strong burn-in observed for reference devices. Moreover, the capacitance-frequency (C-f) plots shows a gradual increase in the capacitance at frequencies below 100 Hz (**Figure S8**). According to Xu et al., this behavior is attributed to the presence of deep defect states. [28] Conversely, the vitamin C interlayer devices shows a flat response, indicating a low presence of deep defect states.
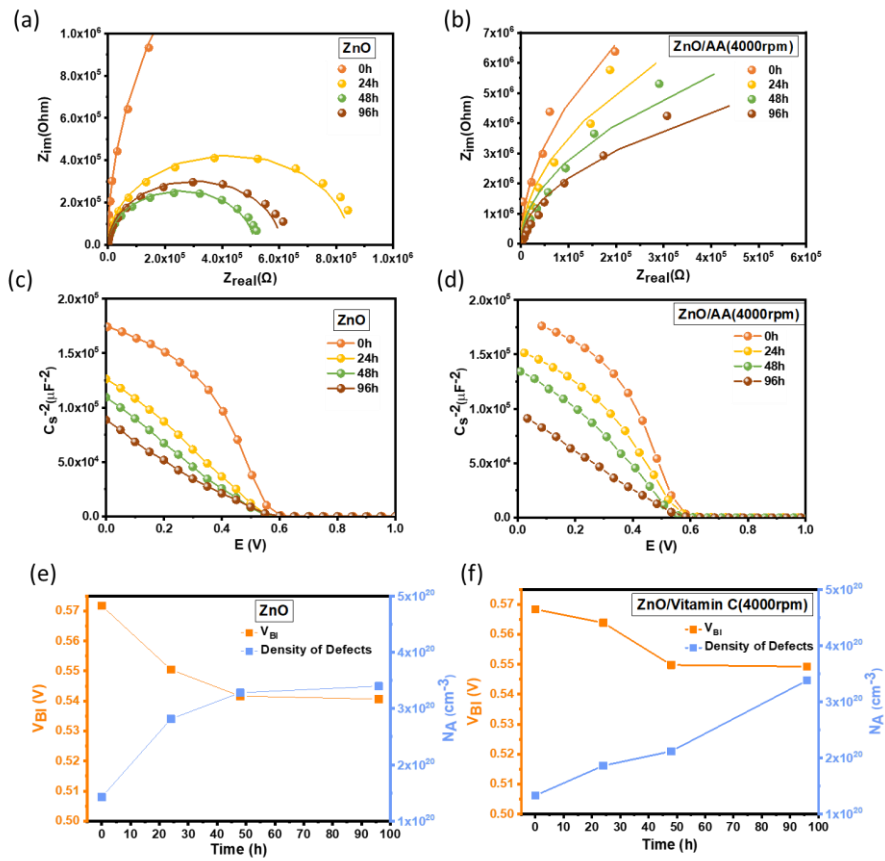

Figure 5. (a, b) Nyquist plots; (c, d) Capacitance as a function of applied voltage at 10 kHz; (e, f) built-in voltage (V_{BI}) and density of defects (N_A), of reference PBDBT:IT-4F devices containing a pure ZnO as ETL and devices containing a Vitamin C interlayer between the active layer and ZnO (ZnO/vitamin C), under exposure to 1 Sun AM 1.5G irradiation.

Table 3: Parameters of fitted data using the equivalent circuit and capacitance measurements.

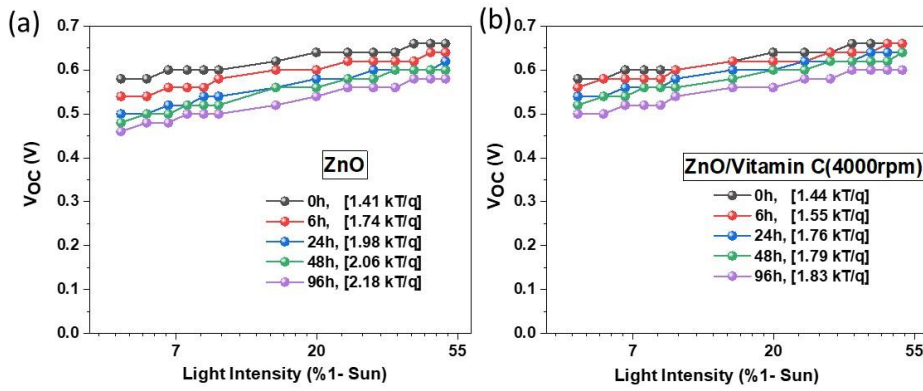| Time (h)	R_{rec} (kΩ)	V_{BI} (V)	N_A (cm^{-3})	R_{rec} (kΩ)	V_{BI} (V)	N_A (cm^{-3})
0	6570	0.572	1.43×10^{20}	2.22×10^5	0.568	1.33×10^{20}
24	849	0.549	2.86×10^{20}	1.28×10^5	0.564	1.86×10^{20}
48	571	0.542	3.25×10^{20}	7.61×10^4	0.550	2.23×10^{20}
96	605	0.540	3.40×10^{20}	4.80×10^4	0.549	3.44×10^{20}

Figure 6. Light-intensity dependent V_{OC} (expressed as the percentage of 1 Sun irradiation) for (a) reference, and (b) devices with vitamin C interlayer, under exposure to 1 Sun AM 1.5G irradiation for increasing time intervals.

Light-intensity dependent measurements were performed to further understand the impact of vitamin C interlayer on the charge recombination. First, we examined the J_{sc} variation under different light intensities. In general, J_{sc} directly depends on the light intensity, as described by the following relationship: $Jsc \propto P_{in}^{\alpha}$; where α equal to unity is the signature of no bimolecular recombination. As shown in **Figure S9**, both reference and devices with vitamin C interlayer show a linear dependence of J_{sc} to light intensity, implying weak bimolecular recombination.[29] Subsequently, we examined the relationship between Voc and light intensity, as shown in **Figure 6**. Generally, Voc is directly related to $\ln(P_{in})$ n $k_B T/q$, where P_{in} is the light intensity, n the ideality factor, k_B the Boltzmann constant, T the absolute temperature, and q the elementary charge. It is generally considered that if the slope value is close to $k_B T/q$, the bimolecular recombination dominates, while for the slope values near 2 $k_B T/q$, the trap-assisted recombination dominates.[29] As shown in **Figure 6a**, the slope value

of reference devices increases over 96 h of light exposure from 1.41 k_BT/q to 2.18 k_BT/q, while that of devices containing vitamin C interlayer decreases less (from1.44 k_BT/q to 1.84 k_BT/q). This indicates a suppression of trap-assisted charge recombination in devices containing vitamin C interlayer, as compared to the reference devices. This is consistent with the degradation of ITIC molecules at the ZnO interfaces, due to photocatalytic reactions, leading to increased charge carrier accumulation and recombination close to that interface.

Conclusion

In summary, we have demonstrated that vitamin C employed as an interlayer between ZnO ETL and the active layer can greatly improve the photostability of NFA OSC. After 96 h of continuous photodegradation under 1 Sun, devices containing vitamin C interlayer retain 63 % of their original value, while reference devices retain only 38 %. The major reason for this stabilization can be found in the capability of vitamin C to act as an antioxidant, which scavenges the radicals formed in the photocatalytic decomposition of the active layer molecules facilitated by ZnO electron transport layer. The application of naturally occurring antioxidants for interface materials, as demonstrated in this work, brings us one step closer towards the realization of fully green, bio-based and stable high-efficiency organic solar cells for commercial applications.

Experimental Section

Materials: L-ascorbic acid ($\geq$ 99 % purity), chlorobenzene, zinc oxide ink and 1,8-diiodooctane were purchased from Sigma Aldrich. Polymer donor (PBDBT) and non-fullerene acceptor (IT-4F) were purchased from 1-Materials (Canada). All reagents were used as such without further purification.

Device fabrication and Characterization: The patterned ITO-coated glass substrates were sonicated in a soap solution, deionized water, acetone and isopropyl alcohol, each for 15 minutes. The cleaned substrates were UV-ozonized for 30 minutes. After that, ZnO nanoparticles were spin-coated at 3000 rpm for 60 seconds and annealed at 130 °C for 15 minutes. To create the vitamin C interlayer, 2 mg of vitamin C was dissolved in 1 ml of ethanol, and spin-coated with various spin speeds (from 1000 to 4000 rpm) for 60 seconds, and subsequently annealed at 110 °C for 5 minutes. Photoactive layers were deposited from

PBDBT:IT-4F solution in chlorobenzene, in the weight ratio of 1:1. The blend solution was spin-coated at 2500 rpm for 60 seconds (corresponding to the thickness of ≈ 100 nm), and subsequently annealed at 110 °C for 10 minutes. A 10 nm film of MoOx was thermally evaporated as the hole transport layer, followed by a silver contact layer with a thickness of 100 nm (deposition rate 0.05 Å s^{-1}, deposition pressure ≈ 5 x10^{-7} Torr). The current density–voltage (J-V) measurements were recorded using ABET technology solar simulator (class AAA) under 1 Sun condition with the intensity of 100 mW cm^{-2}. EQE measurements were carried out using Bentham TMc 300 Monochromator. Stability tests were performed using a home-built controllable automatic measurement setup and an infinityPV ISO Sun solar simulator lamp, under open circuit conditions. UV-vis absorption spectra of the thin films were recorded using a UV-2700 Shimadzu, in the wavelength range 330-830 nm. Impedance spectra were measured in dark using Biologic SP-150e.

Supporting Information

Supporting information is available from the Wiley Online Library or the authors.

Keywords

antioxidant, ascorbic acid, vitamin C, organic solar cells, recombination, photostability, non-fullerene acceptors, ZnO, IT-4F, PBDBT, interlayer, ETL

References

[1] a) L. W. T. NG, S. W. Lee, D. W. Chang, J. M. Hodgkiss, D. Vak, *Adv.Mater. Technol.* **2022**, 2101556. b) F. M. v. d. Staaij, I. M. v. Keulen, E. v. Hauff, *Sol. RRL.* **2021**,5, 2100167. c) H. Meddeb, M. G-Köhler, N. Neugebohrn, U. Banik, N. Osterthun, O. Sergeev, D. Berends, C. Lattyak, K. Gehrke, M. Vehse, *Adv. Energy Mater.* **2022**, 12, 2200713.

[2] a) Y. Cui, L. Hong, and J. Hou, *ACS Appl. Mater. Interfaces* **2020**, 12, 38815−38828. b) Y. J. Kim, S. Eun Park , B. J. Cho, *Nano Energy.* **2022**, 93, 106775. c) M. Jahandar, S. Kim, D. C. Lim, *ChemSusChem* **2021**,14, 3449. d) Z. Li, T. Ma, H. Yang, L. Lu, R. Wang, *Sol. RRL*, **2021**, 5, 2000614. e) M. Hatamvand et.al, Nano Energy, **2020**, 71, 104609. f) E. Ravishankar et.al, Cell Reports Physical Science, **2021**, 2, 100381.

[3] a) L. Zhu, M. Zhang, J. Xu et al, *Nat. Mater.* **2022,** 21, 656. b) W. Gao, F. Qi, Z. Peng et al, *Adv. Mater.* **2022**, 34, 2202089. c) J. Wang, Z. Zheng, Y. Zu et al, *Adv. Mater.* **2021**, 33, 2102787.d) Y. Cui, Y. Xu, H. Yao, et.al *Adv.Mater.* **2021**, 33, 2102420. e) G. Zhang, J. Zhao, P. C. Y. Chow, K. Jiang, J. Zhang, Z. Zhu, J. Zhang, F. Huang, H. Yan, *Chem. Rev.* **2018**, 118, 3447.

[4] a) P. Cheng, X. Zhan, *Chem. Soc. Rev.*, **2016**, 45, 2544. b) S. Rafique, S. M. Abdullah, K. Sulaiman, M. Iwamoto, *Renewable and Sustainable Energy Reviews* **2018**, 84, 43. c) M. Jørgensen, K. Norrman, S. A. Gevorgyan, T. Tromholt, B. Andreasen, F. C. Krebs, *Adv.Mater.* **2012**, 24, 580. d) W. Greenbank et.al., Energy Technol. **2020**, 8, 2000295. e) B. Arredondo et.al., Solar Energy, **2022**, 232,120.

[5] a) S. Cros, R. de Bettignies, S. Berson, S. Bailly, P. Maisse, N. Lemaitre, S. Guillerea, *Solar Energy Materials & Solar Cells*. **2011**, 95, S65. b) Luke J. Sutherland, H. C. Weerasinghe, G. P. Simon, *Adv. Energy Mater.* **2021**, 11, 2101383. c) B. Arredondo et.al., ACS Appl. Energy Mater, 2020, 3, 6476. d) E. Destouesse, M. Top, J. Lamminaho. H.-G. Rubahn, J. Fahlteich, M. Madsen Flexible and Printed Electronics 2019, 4, 045004

[6] a) W. R. Mateker, M. D. McGehee, *Adv. Mater.* **2017**, 28, 1603940. b) W. R. Mateker, I. T. Sachs-Quintana, G. F. Burkhard, R. Cheacharoen, M. D. McGehee, *Chem. Mater.* **2015**, 27, 404. c) Y. Che, M. R. Niazi, R. Izquierdo, D. F. Perepichka, *Angew. Chem. Int. Ed.* **2021**, 60, 24833. d) V. Turkovic, S. Engmann, D. A.M. Egbe, M. Himmerlich, S. Krischok , G. Gobsch, H. Hoppe, Solar Energy Materials & Solar Cells, **2014**, 120, 654. e) L. Ciammaruchi et al., J. Mater. Res., **2018**, 33, 1909.

[7] a) X. Du, T. Heumueller, W. Gruber, A. Classen, T. Unruh, N. Li, C. J. Brabec, *Joule*, **2019**, 3, 215. b) Y. Jiang, L. Sun, F. Jiang, C. Xie, L. Hu, X. Dong, F. Qin, T. Liu, L. Hu, X. Jiang, Y. Zhou, *Mater. Horiz.,* **2019**, 6, 1438. c) S.Park, H. J. Son, *J. Mater. Chem. A*, **2019**, 7, 25830.

[8] a) C. Liu, C. Xiao, W. Li, *J. Mater. Chem. C*, **2021**, 9, 14093. b) Z. Yin, J. Wei, Q. Zheng, *Adv.Sci.* **2016**, 3, 1500362.

[9] a) P. Jiang, L. Hu, L. Sun, Z. Li, H. Han, Y. Zhou, *Chem. Sci.*, **2022**, 13, 4714. b) A. Azeez, K. S. Narayan, *J. Phys. Chem. C.,* **2021**, 125, 12531.

[10] L -Y. Su, H -H. Huang, C -E. Tsai et al., *Small*, **2022**, 18, 2107834.

[11] L. Hu, Y. Jiang, L. Sun, C. Xie, F. Qin, W. Wang, Y. Zhou, *J. Phys. Chem. Lett*. **2021**, 12, 2607.

[12] B. Liu, Y. Han, Z. Li, H. Gu, L. Yan, Y. Lin, Q. Luo, S. Yang, C -Q. Ma, *Sol. RRL*. **2021**, 5, 2000638.

[13] X. Xu, J. Xiao, G. Zhang, L. Wei, X. Jia, H -L. Yip, Y. Cao, *Science Bulletin*. **2020**, 65, 208.

[14] a) V. Turkovic, S. Engmann, N. Tsierkezos, H. Hoppe, M. Madsen, H. G. Rubahn, et al., Appl. Phys. A: Mater. Sci. Process., 2016, 112, 255. b) V. Turkovic, S. Engmann, N. Tsierkezos, H. Hoppe, U. Ritter, G. Gobsch, *ACS Appl. Mater. Interfaces*, **2014**, 6, 18525. c) V. Turkovic, S. Engmann, N. Tsierkezos, H. Hoppe, M. Madsen, H. G. Rubahn, et al., *J. Phys. D: Appl. Phys*., **2016**, 49, 125604.

[15] V. Turkovic, M. Prete, M. Bregnhøj et.al, *ACS Appl. Mater. Interfaces.* **2019**, 11, 41570.

[16] M. Prete, E. Ogliani, M. Bregnhøj et.al, *J. Mater. Chem. C*, **2021**, 9, 11838.

[17] a) J. Oh, S. M. Lee, S. Jung, J. Lee, G. Park, S -H. Kang,Y. Cho, M. Jeong, B. Lee, S. Kim, C. Yang, *Sol. RRL*., **2021**, 5, 2000812. b) J. Guo, Y. Wu, R. Sun, W. Wang et.al, *J. Mater. Chem. A*, **2019**, 7, 25088.

[18] a) D.E. Cabelli, B.H.J. Bielski, J. Phys. Chem., **1983** 87, 1809. b) R. A. Larson, Naturally occurring antioxidants, CRC-Press; 1st edition, Boca Raton, **1997**.

[19] E. M. Speller et.al, ACS Energy Lett. **2019**, 4, 846.

[20] A. Bendich, L.J. Machlin, O. Scandurra, G.W. Burton, D.D.M. Wayner, Advances in Free Radical Biology & Medicine, **1986**, 2, 419.

[22] S. Trost, K. Zilberberg, A., Behrendt et.al, *Adv. Energy Mater.* **2013**, 3, 1437.

[23] M. Prosa, M. Tessarolo, M. Bolognesi et.al, *ACS Appl. Mater. Interfaces,* **2016**, 8, 1635.

[24] C. B. Ong, L. Y. Ng, A. W. Mohammad, Renewable and Sustainable Energy Reviews, 2018, 81, 536-551.

[25] a) U. Dettinger et.al, Chem. Mater. **2015**, 27, 2299. b) I. Fraga Domínguez, et.al., J. Phys. Chem. C, 2015, 119, 2166. c) J. Razzell-Hollis, J. Wade, W. Chung-Tsoi, Y. Soon, J. Durrant, J-S. Kim, J. Mater. Chem. A, **2014**, 2, 20189. d) Tournebize et al. Adv. Energy Mater. **2016**, 3, 478. e) A. Tournebize et al., Solar Energy Materials & Solar Cells, **2016**, 155, 323.

[26] a) D. G. Romero, L. D. Mario, G. Portale, M. A. Loi, *J. Mater. Chem. A*, **2021**, 9, 23783. b) H-S. Pang, H. Xu, C. Tang, L-K. Meng, Y. Ding, J. Xiao, R-L. Liu, Z-Q. Pang, W. Huang, *Organic Electronics*, **2019,** 65, 275. c) J. T. Heath, J. D. Cohen, W. N. Shafarman, *J. Appl. Phys*. **2004**, 95, 1000. d) J. A. Carr, S. Chaudhary, Appl. Phys. Lett., 2012, 100, 213902.

[27] H-S. Pang, et.al., Organic Electronics, **2019**, 65, 275.

[28] L. Xu, J. Wang, J. W. P. Hsu, PHYSICAL REVIEW APPLIED **2016**, 6, 064020.

[29] N. Gasparini, M. Salvador, S. Fladischer et.al, *Adv. Energy Mater.* **2015**, *5*, 1501527.